Investigation of Dynamic Viscosity of Several Aliphatic and Aromatic Hydrocarbons in Connection with Thermo-Occupancy Function

F. Sahin-Dinc*

Karadeniz Technical University, Surmene Abdullah Kanca Vocational School, Machinery and Metal Technologies, Machinery Department, 61530, Camburnu, Surmene, Trabzon, Turkey

Received: 15.01.2022 & Accepted: 31.01.2022

Doi: 10.12693/APhysPolA.141.535 *e-mail: fatmadinc@ktu.edu.tr

In the current study, the Newtonian viscosity-hole fraction correlation has been extended to predict the dynamic viscosity η of pure aliphatic and aromatic hydrocarbon liquids for temperatures between 298.15 and 473.15 K and pressures up to 201.9 MPa. The correlation implicates the thermo-occupancy function $Y_h = Y_h(h, T)$ in terms of T and the function of $h = h(P, T)$ reckoned by the Simha–Somcynsky equation of state. The uncertainties for the measurements were estimated to be less than 0.16% regarding the specific volume. Dynamic viscosity prediction was performed in two approaches, one of which includes the additional hole fraction parameter h'. The fitting results of the equations with and without h' were in this report determined to be from 0.09 to 0.26% and 0.31 to 0.53%, respectively. It was found that both the volumetric and viscosity characterisation indices examined were related to the molecular conformation and architecture.

topics: dynamic viscosity, hole fraction, Simha–Somcynsky (SS), aromatics

1. Introduction

Academic and industrial interests in hydrocarbon fluids are still attractive since they are the base source for many industrial processes. The knowledge of transport properties of hydrocarbons, particularly viscosity, plays an important role in chemical and petroleum engineering disciplines such as the operation, design and sizing of pipes, accessories, chemical and transport equipment, as well as in the simulation and optimisation of control processes. In particular, the trend of aliphatics and aromatics for viscous behaviour under high temperature and high pressure (HTHP) conditions results from the tendency of the utilization of deeper hydrocarbon reserves in the oil industry. Despite the apparent significance of hydrocarbon viscosity in the petroleum industry, there is still an experimental data shortage for heavy hydrocarbons and aromatics under HTHP conditions [1, 2]. Direct viscosity measurements for the hydrocarbon fluids encountered specifically under HTHP conditions with desired precision are difficult and sometimes not feasible because of the laboratory measurement cost, taking up a great deal of time and unavailability of liquid hydrocarbon samples, etc. Therefore, it is highly desirable to use theoretical approaches to estimate the accurate viscosity of hydrocarbons within the entire temperature and pressure ranges.

Throughout the past fifty years, there have been continual advances toward modelling viscosity in terms of free volume concept. This method usually needs an equation of state (EoS) and preferably incorporates a free volume parameter. For more than a half century, the Simha–Somcynsky equation of state (SS-EoS) has indicated great prospects regarding the precise modelling of density data, not only for pure substances or compounds but also for complex fluids and their blends at reduced pressures and HTHP conditions [3, 4]. A few more recent studies concerning viscosity equation coupled with SS-EoS as follows. Utracki provided new reference correlations for the free volume and viscosity by using a modified Doolittle formula [5] for many forms of organic components including normal alkanes (n-alkanes) [6], mixtures of n-alkanes [4], polymers [7–9], oligomers and polymers [10]. In an attempt to develop an accurate model for viscosity in connection with the SS-EoS for some molten polymers (ABS, PP, PS), Kadijk and van den Brule [11] modified the correlation of Utracki et al. [10, 12]. They incorporated the term temperature into the viscosity model, which was previously posited in several contributions [10, 12]. Another approach, concerning the free volume-viscosity model, was analysed by Sedlacek et al. [13]. They modified Utracki's approach in conjunction with the Simha-Somcynsky (SS) theory to attain uniform and

smooth master curves in regard to the linearisation of viscosities at zero shear and constant stress for the examined polymer liquids. Rojo et al. [14] focused on the explanation of viscosity in connection with SS-EoS for isotactic and syndiotactic polypropylenes using the modified viscosity equation described by Sedlacek et al. [13]. In a subsequent effort Sorrentino and Pantani [15] combined the Newtonian viscosity described in the Doolittle approach [5] with the SS-EoS for atactic and syndiotactic polystyrene regarding the viscosity-free volume relationship. Yahsi [16] applied Utracki's viscosity model for linear alkanes and modified it for three-branched alkanes. Yahsi [17] and Yahsi and Sahin [18] proposed a generalised model in conjunction with the SS-EoS for straight chain, ramified high molecular weight hydrocarbons and ring attached hydrocarbons (cycloalkanes) up to C_{18}, C_{38}, and C_{26}, respectively, up to elevated pressure of 350 MPa and temperature of 408 K. Sahin et al. [19] further employed Newtonian viscosity modelling and correlation for the binary mixtures of high molecular weight branched alkanes with known composition through the concept of hole fraction. In recent publications, Sahin-Dinc [20], Dinc et al. [21], and Sahin-Dinc et al. [22, 23] posited a viscosity model formulated in relation to the Simha–Somcynsky hole theory to correlate the viscous effect to free volume of polymer melts for both shear and elongational flow.

A recently developed physically-based scheme has been described for molecular transport of aliphatics (including pure short- and long-chain n-alkanes and branched alkanes), cycloalkanes (naphthenes) and their mixtures, as stated earlier. Now it is further utilised for the prediction of viscosity in terms of hole fraction of two dissimilar chemical classes, specifically straight-chain alkanes (n-alkanes) and aromatics with single and double rings, for the latter of which the model has not been tested at a wide range of conditions. The current work is revolved particularly around reducing gaps in the accessible viscosity measurements for aromatics at HTHP. To the best of our knowledge, considerably few measured rheological values have been reported on 1,3-dimethylbenzene (meta-xylene), 1,2,3,4-tetrahydronaphthalene (tetralin), and 1-methylnaphthalene (1-MNP) at pressures above atmospheric [1, 24–28] specifically under conditions of HTHP [2, 29] and there are only limited theoretical studies reported on the correlation of viscosity-free volume concerning these chemical species [28–30]. As far as we are aware, the parameters of the zero shear viscosity model and SS theory are the first to be reported for the concerned aromatics both at atmospheric and elevated pressure.

The intent of the current treatise is to present the results of the Newtonian model that provides an opportunity to couple with SS-EoS by means of a thermo-occupancy function comprising temperature and hole fraction. More precisely, to compare the viscosity values returned by this model with the measured data is one of the aims. In addition to that, an important focus is on examining the relation between Newtonian viscosity and the parametric quantities of the statistical thermodynamic equation of state (SS-EoS) specifically the vacancy fraction for some aromatic hydrocarbons and, for comparison purposes, for some n-alkanes (acyclic hydrocarbons) at temperatures range of $T = 298.15$–473.15 K and for pressures up to 200 MPa. Four n-alkanes (C_8, C_{10}, C_{12}, C_{18}) and three aromatic hydrocarbons (1,3-dimethylbenzene (meta-xylene), 1,2,3,4-tetrahydronaphthalene (tetralin), and 1-methylnaphthalene (1-MNP)) are the liquid samples under investigation.

2. Theories

2.1. A brief summary of Simha and Somcynsky lattice–hole model

The widely known Simha–Somcynsky hole theory [31] visualised the disordered structure of fluids as an ensemble of cells of equal size, in which a fraction y is filled (occupied) with molecular segments, whereas the remaining parts, $h = 1 - y$, are left unfilled with holes on the quasi-lattice. The fraction of h is given with the relation $h = N_h/(N_h + sN)$, where N_h and sN stand for the number of holes and occupied cells, respectively. The measure of molecule number is N, and s identifies the number of segments per molecule placed in a quasi-lattice. These segments usually correspond to the measure for the carbon atom numbers within the chemical backbone chain specifically, and they may not be similar to the repeating unit of liquids.

The theory allows us to compute the optimum hole fraction h from a numerical solution of the Helmholtz free energy differentiations. The differential, $P = -(\partial F/\partial V)_T$, refers to the conventional thermodynamic pressure definition where F stands for the free energy and is minimized as $(\partial F/\partial y)_{V,T} = 0$ at thermodynamic equilibrium. Thus the dimensionless SS-EoS is formulated in the following coupled expressions

$$\begin{cases} \frac{\tilde{P}\tilde{V}}{T} = \frac{1}{Q-1} + \frac{2}{T}\frac{y}{(y\tilde{V})^2}\left[\frac{A}{(y\tilde{V})^2} - B\right] \\ \\ \frac{s}{3c}\left[\frac{\ln(1-y)}{y} + \frac{s-1}{s}\right] = \\ \quad \frac{3Q-1}{3(1-Q)} + \frac{1}{6T}\frac{y}{(y\tilde{V})^2}\left[2A - \frac{3B}{(y\tilde{V})^2}\right]. \end{cases} \quad (1)$$

Here, the total external freedom degree of the molecule $3c$ and the segment number s are linked with the fraction $3c/s$ appearing explicitly in the equilibrium condition above. It is used in reference to chain flexibility. The constants $Q{=}y/(\sqrt{2}\,y\tilde{V})^{1/3}$, and $A{=}1.011$ and $B{=}1.2045$, are dimensionless quantities corresponding to the closest adjacent interaction centres in the close packing as the

cell geometry. The dimensionless reduced pressure, volume and temperature variables are represented by $\tilde{P}$, $\tilde{V}$, and $\tilde{T}$, respectively, and indicate the commonality of behaviour for all liquids in the given system. These quantities are reduced through the P^*, V^*, and T^* material-dependent reducing parameters as $\tilde{P} = P/P^*$, $\tilde{V} = V/V^*$, and $\tilde{T} = T/T^*$. The reducing quantities are joined in a single equation $P^*V^*m_0/T^* = cR/s$, where R stands for the universal gas constant, and m_0 is the molar segmental mass. In relation to the Lennard–Jones (L–J) scaling molecular quantities ε^* and υ^*, the scaling variables can be further expressed as $P^* = q_z\varepsilon^*/(s\upsilon^*)$, $V^* = N_\mathrm{A}\upsilon^*/m_0$, and $T^* = q_z\varepsilon^*/(ck)$. Here N_A symbolises the Avogadro's number, and k_B is the Boltzmann constant. The maximum characteristic segment-segment interaction energy is denoted by ε^*, and υ^* is identified as the intersegmental characteristic hardcore volume. A measure for the total surface coordination number among s segments is expressed as $q_z = s(z-2)+2$, where z corresponds to the ligancy of fcc (face-centred cubic) fixed at $z = 12$.

The SS-EoS provides the description of the PVT surface and, ultimately, the prediction of vacancy fraction, $h = h(V,T)$ or $h = h(\tilde{V},\tilde{T})$, from experimental PVT measurements. Having h values at hand not only yields the analysis of various equilibrium processes and transport properties of fluids, but also permits the association of equilibrium processes to transport properties or vice versa [6, 9–11, 15, 17–23, 32–36].

2.2. Interpretation of viscosity characterisation of liquid hydrocarbons

Eyring significant structure theory (ESS) provides the link between the transport and thermodynamic properties of liquids [37, 38]. According to this theory, if the $(1-h)$ fraction of the shear plane is occupied with quasi-solid and the remaining fraction h is filled up with quasi-gas molecules, then the viscosity becomes [37, 38]

$$\eta = (1-h)\,\eta_s + h\eta_g, \tag{2}$$

where η_s and η_g refer to the viscosities for the quasi-solid and quasi-gas molecules, respectively. The quasi-gas part (unoccupied) viscosity $h\eta_g$ is insignificantly low compared to the quasi-solid part (occupied) viscosity $(1-h)\eta_s$ and, therefore, $h\eta_g$ can be neglected. Hence the viscosity of quasi-solid molecules is considered to be the viscosity of liquid written as [17, 18]

$$\eta_{sp} = (1-h)\,\eta_s, \tag{3}$$

where η_{sp} refers to the solid part viscosity.

In a Newtonian flow, the dynamic viscosity comprising the Eyring strain rate is expressed as a function of temperature by Yahsi [17] and Yahsi and Sahin [18] as

$$\eta_N = \frac{3\sqrt{2}\,s}{q_z h}\frac{k_\mathrm{B}T}{k'\,\upsilon}. \tag{4}$$

In (4), k_B is referred to as the Boltzmann constant, and the segmental molar volume is denoted by υ. The portion of $q_z h/s$ is a measure of the number of the available contiguous vacant sites. The Eyring jumping frequency k' of a segment that slips past the neighbouring molecules over the energy barrier per second is given by [39–41]

$$k' = \kappa\,\frac{k_\mathrm{B}T}{h_p}\,\frac{Z^*}{Z}\,\exp\left(-\frac{E_a}{k_\mathrm{B}T}\right), \tag{5}$$

where κ denotes the transmission coefficient, which is a measured probability of an activated complex moving into a vacant site. In (5), and h_p is the Planck constant. The flow-activation energy of a segment required for jumping, E_a, corresponds to the energy barrier between one equilibrium position in the liquid and the next, given by

$$E_a = \frac{E_s}{h} = \frac{1-h}{2h}\,a' q_z\,\Phi, \tag{6}$$

where E_s is the sublimation energy, and Φ characterizes the Lennard–Jones potential energy resulting from the interaction between a pair of segments. The activation energy proportionality constant is denoted by a'.

In this study, the Eyring theory [39, 42] is modified by the assumption that one of the vibrational modes in an equilibrium condition has been transformed into a translational state in an activated mode during flow. There is no transition in the translational and rotational freedom degrees between the normal and activated states. In (5), the fraction Z^*/Z for a molecule signifies the ratio of the partition function, being in the flow-activated condition to that at equilibrium, and is then given as follows

$$\frac{Z}{Z*} = \frac{\exp\left(-\frac{h_p\nu}{2k_\mathrm{B}T}\right)}{1-\exp\left(-\frac{h_p\nu}{k_\mathrm{B}T}\right)}, \tag{7}$$

where ν refers to the frequency of a molecule vibrating in the normal mode.

In the formulation of (4), it can be assumed that the Newtonian viscosity is the same as the solid-like viscosity of a liquid in (3). The viscosity formulation is obtained by replacing the Newtonian viscosity in (4) with the solid-like viscosity in (3) using (5), (6) and (7) [17, 18]

$$\ln\left(\frac{h}{1-h}\,\frac{1-\mathrm{e}^{-h_p\nu/(k_\mathrm{B}T)}}{\mathrm{e}^{-h_p\nu/(2k_\mathrm{B}T)}}\,\eta_{sp}\upsilon\right) = \ln(\eta^*) + \frac{1-h}{h}\,\frac{\alpha}{T}. \tag{8}$$

In (8), the right-hand side is referred to as the logarithm of zero-shear viscosity, $(\ln\eta_0)$, i.e.,

$$\ln(\eta_0) = \ln(\eta^*) + \frac{1-h}{h}\,\frac{\alpha}{T}. \tag{9}$$

In a scaled form, (9) becomes

$$\ln(\tilde{\eta}_0) = \frac{1-h}{h}\,\frac{\alpha_s}{\tilde{T}}. \tag{10}$$

Here, $\tilde{\eta}_0 = \eta_0/\eta^*$ is the scaled quantity in which η^* is the viscosity extrapolation at the highest hole fraction value. In (9) and (10), α and α_s are

measures of activation energy and are presumably affected by the segmental friction, molecular structure, branching, composition, additives, etc. These parameters (the expressions for η^*, α, and α_s, respectively), are given as follows:

$$\eta^* = \frac{3\sqrt{2}N_{\mathrm{A}}sh_p}{q_Z\,\kappa}, \quad \alpha = a'\,\frac{q_Z\,\Phi}{2k_{\mathrm{B}}},$$

$$\alpha_s = a''\frac{q_Z\,\Phi}{2k_{\mathrm{B}}T^*}. \tag{11}$$

Here, a' and a'' stand for the activation energy coefficients, and the function Φ changes slowly with respect to temperature and pressure [17–19].

A ratio of the fraction $\frac{y}{h}$ to absolute temperature T in (9), and scaled temperature $\tilde{T}$ in (10) is called *thermo-occupancy* function and represented, respectively, by [20–23]

$$Y_h = \frac{1-h}{h}\,\frac{1}{T} \tag{12}$$

and

$$\tilde{Y}_h = \frac{1-h}{h}\,\frac{1}{\tilde{T}}. \tag{13}$$

The thermo-occupancy function Y_h not only provides the thermodynamic properties of liquids obtained from the equilibrium condition of the SS-EoS but also constructs a bridge between equilibrium and transport properties through the viscosity equation defined in (9). In order to linearize the dependence between two quantities, namely hole fraction and dynamic viscosity (see (9)), an empirical additive hole fraction parameter, h', is defined [17, 18]. With the inclusion of parameter h', (9) and (10) becomes

$$\ln(\eta_0) = \ln(\eta^*) + \frac{1-h}{h+h'}\,\frac{\alpha}{T}, \tag{14}$$

$$Y_h = \frac{1-h}{(h+h')}\,\frac{1}{T}, \tag{15}$$

and

$$\ln(\tilde{\eta}_0) = \frac{1-h}{h+h'}\,\frac{\alpha_s}{\tilde{T}}, \tag{16}$$

$$\tilde{Y}_h = \frac{1-h}{(h+h')}\,\frac{1}{\tilde{T}}. \tag{17}$$

Since (14) and (15) includes an additive hole fraction term h' necessary for the flow, it corresponds to the transport state of the model. However, (9) represents the equilibrium state of the model. The estimation of viscosity from volumetric measurements, and vice versa, can be obtained through (14)–(17).

The "viscoholibility", a combined word of hole fraction and viscosity, is expressed as the differentiation of $\ln(\eta_0)$ in (9) and (14) with respect to vacancy fraction at a constant absolute temperature [20–23]

$$\left.\frac{\partial \ln(\eta_0)}{\partial h}\right|_T = -\frac{\alpha}{h^2T}, \tag{18}$$

where the sign "−" indicates the inverse relationship between zero-shear viscosity and hole fraction.

3. Calculations and discussion

3.1. The PVT data fit through the SS theory (SS-EoS Fits)

The PVT data of hydrocarbon fluids examined in this work were provided by Caudwell et al. [2, 43] in the temperature range 298.15–473.15 K and for the range of pressures from 0.1 to 202.4 MPa. The density is determined with the aid of a steady-state vibrating-wire instrument, technical details of which are provided in [2, 43].

The density data of two different chemical families were evaluated in this study. The candidate liquid hydrocarbons examined were four n-alkanes ($\mathrm{C}_n\mathrm{H}_{2n+2}$); n-octane, n-decane, n-dodecane, n-octadecane, (C_8, C_{10}, C_{12}, and C_{18}) and three aromatic hydrocarbons; 1,3-dimethylbenzene (meta-xylene), 1,2,3,4-tetrahydronaphthalene (tetralin) containing cyclohexene and a benzene ring, and 1-methylnapthalene (1-MNP) with two aromatic rings (displayed in Fig. 1). Mono-aromatic hydrocarbons ($\mathrm{C}_n\mathrm{H}_{2n-6,-8,-10}$) are m-xylene and tetralin, while 1-MNP is a di-aromatic hydrocarbon ($\mathrm{C}_n\mathrm{H}_{2n-12,-14,-16}$).

The Simha–Somcynsky (SS) EoS (1) were used as the PVT inputs to the zero shear viscosity model. The Mathematica program was composed to pursue the fits and quantify the SS theory measures: V^*, T^*, and P^*. These parameters must have values for the structural flexibility quantity $3c/s$ and the Lennard–Jones interaction quantities (υ^* and ε^*) together with $h = h(\tilde{P}, \tilde{T})$ to estimate the viscosity and its derivation. In the structural flexibility parameter $3c/s$, the evaluation parameter c is taken as a disposable quantity, and the chain length s corresponds to the sum of carbon numbers and the values assigned for each ring structure. The corresponding s values for benzene and cyclohexene ring structures are set to be 6.6 and 5.3, respectively [18].

For the simultaneous assessment of the entire data set, N number of equations in terms of V^* and T^* are derived by projecting the measured N number of measured PVT data on the theory. Here P^* is introduced in reference to reducing parameters V^* and T^* for a given c and determined s values. Each equation is expanded up to the first power and worked out for the unidentified V^* and T^* parameters by adopting the "pseudo-inverse matrix technique". With the computed V^* and T^*,

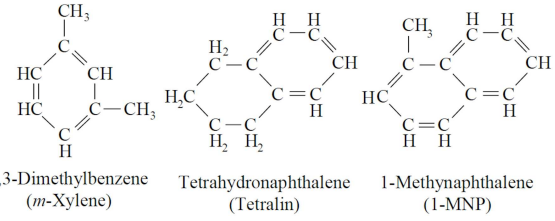

Fig. 1. Structural formulas of aromatics.

TABLE I

Materials' characteristics of hydrocarbons under study.

Hydrocarbons	Hill (emprical) formula	MW [g/mol]	Temp. range[a] [K]	Pressure range[b] [MPa]
n-octane	C_8H_{18}	114.224	298.15–473.15	0.1–201.9
n-decane	$C_{10}H_{22}$	142.276	298.15–373.15	0.1–191.7
n-dodecane	$C_{12}H_{26}$	170.328	298.15–473.15	0.1–191.7
n-octadecane	$C_{18}H_{38}$	254.484	323.15–473.15	0.1–92.2
1,3-dimethylbenzene (*m*-xylene)	C_8H_{10}	106.16	298.15–473.15	0.1–198.5
1,2,3,4-tetrahydronaphthalene (tetralin)	$C_{10}H_{12}$	132.196	298.15–448.15	0.1–201.9
1-methylnaphthalene (1-MNP)	$C_{11}H_{10}$	142.19	298.15–473.15	0.1–202.4

[a]Temperature range used for PVT and viscosity data. [b]Pressure range used for PVT and viscosity data.

TABLE II

Equation of state materials' characteristics of hydrocarbons.

	n-octane	*n*-decane	*n*-dodecane	*n*-octadecane	*m*-xylene	tetralin	1-MNP
m_0 ($\times 10^3$) [kg]	14.28	14.23	14.19	14.14	16.09	13.35	13.94
s	8	10	12	18	6.6	9.9	10.2
c	0.96	1.32	1.24	1.56	0.94	0.93	0.88
$\langle -\Phi/k^* \rangle$ [K]	189.3	210.7	192.3	192.2	221.1	203.68	211.32
V^* ($\times 10^3$) $\left[\frac{\mathrm{m}^3}{\mathrm{kg}}\right]$	1.3210	1.2763	1.2756	1.2516	1.0927	1.0091	0.9719
T^* [K]	11279	10872.2	13194.3	15634.3	11154.3	15422.6	17411.6
P^* [MPa]	596.61	657.08	626.05	636.62	751.49	893.967	921.804
$\langle v^* \rangle$ ($\times 10^6$) $\left[\frac{\mathrm{m}^3}{\mathrm{mol}}\right]$	18.86	18.16	18.11	17.70	17.58	13.47	13.55
$\langle \varepsilon^* \rangle$ [K]	132.047	140.699	134.106	134.009	154.192	142.01	147.329
ΔV [%]	0.12	0.066	0.16	0.16	0.13	0.11	0.12
$\max \Delta V$ [%]	0.69	0.21	0.62	0.36	0.52	0.37	0.42

the optimal best-fit parameters for the components displayed in Table I were ascertained and gathered in Table II by seeking the minimum relative mean absolute percentage error (rMAPE) between theoretical and measured specific volume. Fitting (1) to PVT data of seven hydrocarbon liquids reveals an rMAPE that differs from 0.07 to 0.16. The rMAPE is calculated for the SS-EoS fits from

$$\Delta V = \frac{1}{N} \sum\nolimits_i \frac{\left| V_i^{\mathrm{exp}} - V_i^{\mathrm{calc}} \right|}{V_i^{\mathrm{exp}}} \times 100\%. \qquad (19)$$

This process also renders the fraction $h(P,T)$ together with material-dependent parameters P^*, V^* and T^*.

The Lennard–Jones average energetic $\langle \varepsilon^* \rangle$ and volumetric $\langle v^* \rangle$ quantities are computed and listed in Table II. The magnitude of $\langle \varepsilon^* \rangle$ ranges from 132.047 to 140.699 for the studied *n*-alkanes and from 142.01 to 154.192 for the aromatics ((mono-(*m*-xylene, tetralin, $C_nH_{2n-6,-8,-10}$) and di-aromatics (1-MNP, $C_nH_{2n-12,-14,-16}$)). The values of $\langle v^* \rangle$, which have the opposite trend to $\langle \varepsilon^* \rangle$ given in Table II, differ from 17.7 to 18.86 for *n*-alkanes and from 13.47 to 17.58 for the aromatics. This implies that aromatics with compact structures yield denser structures and have decreasing effects in free volume. The value of $\langle v^* \rangle$ decreases as the chain length of *n*-alkanes increases since the fluidity steps down, while the fluid contracts because of the decreasing space between the fluid molecules. When comparing the order of the calculated values of the mean characteristic repulsive molar volume $\langle v^* \rangle$ across all four *n*-alkanes, one sees that they are in the sequence of *n*-octane > *n*-decane > *n*-dodecane > *n*-octadecane with the differences between *n*-decane and *n*-dodecane being the least marked. It is also consistent with the findings attained from the characteristic volume (V^*) parameters. The aromatics have lower V^* values than *n*-alkanes since the former have closely packed structures. The value of V^* decreases between *n*-alkanes as the chain length increases, according to the scheme: *n*-octane > *n*-decane > *n*-dodecane > *n*-octadecane. Among the aromatics, these values decrease from mono- to di- aromatics, i.e., *m*-xylene > tetralin > 1-MNP, since the structure becomes more compact. Based on these observations, we can state that $\langle v^* \rangle$ and V^* decrease from *n*-alkanes to aromatics, and vice versa for $\langle \varepsilon^* \rangle$. More specifically, $\langle v^* \rangle$ and V^* decrease from short to long chain length *n*-alkanes and from mono- to di-aromatics.

TABLE III

The slope of h and the values extrapolated at 0°C for h and Y_h at 1 arm for the tested Hydrocarbons.

Hydrocarbons	h at 0°C	The slope of $h(T)$ $(\times 10^{-3})$ $[K^{-1}]$	Y_h $(\times 10^{-3})$ $[K^{-1}]$ at 0°C
n-octane	0.106	0.973	30.2
n-decane	0.102	0.919	31.7
n-dodecane	0.082	0.898	37.8
n-octadecane	0.066	0.805	46.2
1,3-dimethylbenzene (m-xylene)	0.090	0.894	35.7
1,2,3,4-tetrahydronaphthalene (tetralin)	0.065	0.781	49.0
1-methylnaphthalene (1-MNP)	0.052	0.714	60.3

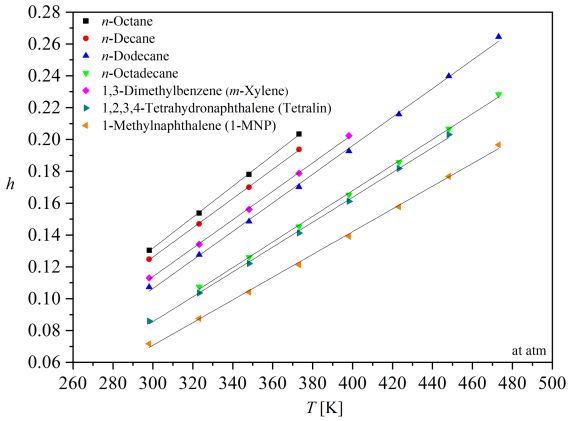

Fig. 2. The computed h (geometrical shapes) vs T at 1 atm with the best fit lines.

Figure 2 is displayed to probe molecular structure effects on hole fraction for the studied hydrocarbons at each T and 1 atm computed from (1). The coloured geometrical shapes symbolise the computed h values and the solid lines refer to the best fit lines through each evaluation set. The computed h findings go up with temperature since the molecules move apart from each other as they gain kinetic energy, and thus free volume ensues.

The values extrapolated at 0°C for fraction h and the slope of the lines in Fig. 2 are listed for each liquid in Table III. For the studied n-alkanes and aromatics, the h values differ and decrease from n-octane to n-octadecane and from mono- to di-aromatics. As the chain length gets higher and the molecule becomes more compact, the free volume decreases, and so does the hole fraction. The same result is obtained for $\langle \varepsilon^* \rangle$ and $\langle v^* \rangle$ analysed above. The material becomes a more tightly packed structure due to the deficiency in vacant defects as a result of having lower v^* and higher ε^*. The slope of the lines (temperature coefficient of hole fraction) also presents the same reduction pattern, going from short to long-chain n-alkanes and from mono- to di-aromatics. Another conclusion from Table III is that the aromatics in the similar temperature and pressure ranges as n-alkanes occupy less volume, so they have less free volume as a vacancy defect and therefore have more viscous behaviour compared to n-alkanes.

Figure 3 illustrates the results shown in Table III as a combined graph of the variation of hole fraction at 1 atm and 0°C and the slope of the lines in Fig. 2 with segment number s. Both h and the slope of h decrease with increasing segment number in Fig. 3a and b, respectively. It means that while the chain

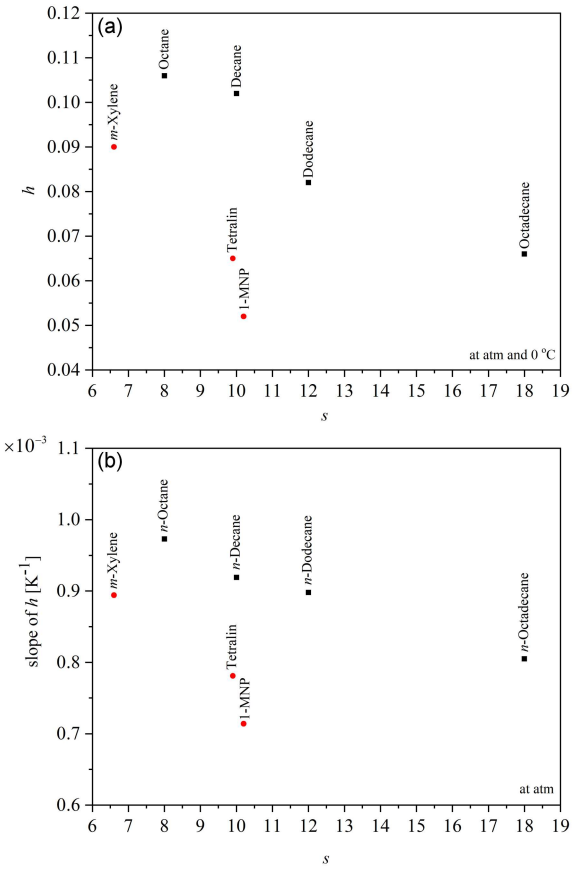

Fig. 3. A combined graph of the variation of h (at 1 atm and 0°C) and the slope of the lines in Fig. 2 at 1 atm with respect to segment number s.

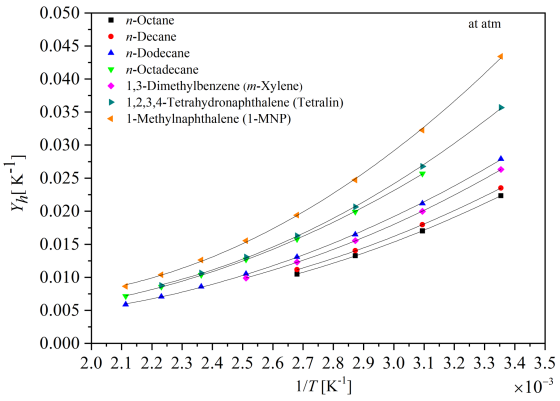

Fig. 4. "Thermo-occupancy function" Y_h vs reciprocal temperature with the best-fit curves.

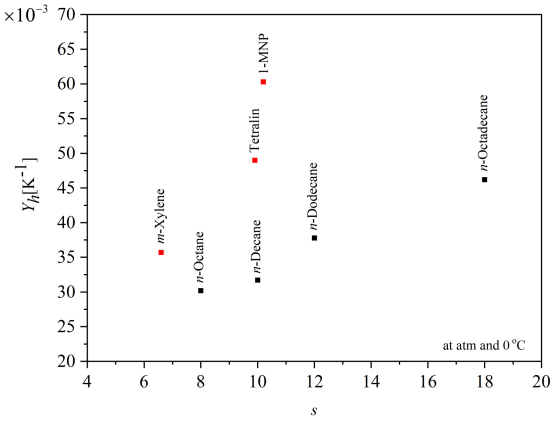

Fig. 5. Dependence of Y_h vs s at 1 atm and 0°C for n-alkanes and aromatics under investigation.

length and the aromaticity (that gives increased stability to the molecule) increase, the fraction h and its slope as a temperature coefficient decrease. It is obvious that values of both h and the slope of h are higher for n-alkanes than that of aromatics with the corresponding segment number since the latter have more stable structures.

The thermo-occupancy function Y_h, for which transport properties are employed, is generated from the SS-EoS model fit. The variations of Y_h of hydrocarbon liquids with reciprocal temperature at ambient pressure are included in Fig. 4. The fits are denoted as the coloured geometrical shapes together with the curves for guiding eyes. The magnitude of Y_h increases as temperature falls for each hydrocarbon in Fig. 4. The changes in the magnitude of Y_h concerning segment number s are depicted in Fig. 5, and the extrapolated Y_h values at 0°C are tabulated for individual hydrocarbons in Table III. It is visible in Fig. 5 that for both chemical groups, Y_h values get higher with the increasing s. The aromatics have higher transportation stability compared to n-alkanes for the corresponding s number. From mono- to di-aromatics, stability steps up as

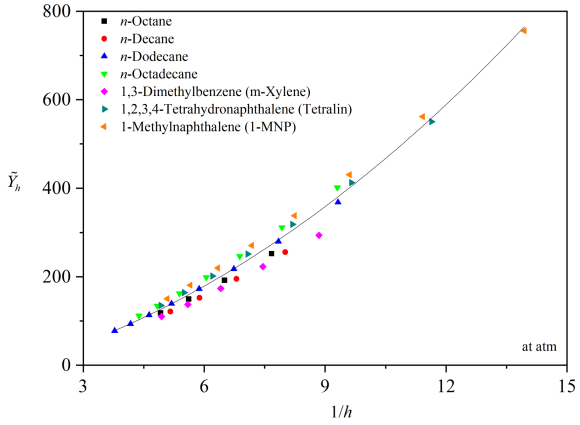

Fig. 6. "Thermo-occupancy function" in a scaled form, $\tilde{Y}_h$, vs $1/h$ at 1 atm.

the molecules are tightly packed with respect to the increased aromaticity. 1-MNP exhibits the highest transportation stability, while n-octane represents the smallest one. The order of the computed values of Y_h for both the examined n-alkanes and aromatics is, respectively, n-octadecane > n-dodecane > n-decane > n-octane and 1-MNP > tetralin > m-xylene.

Figure 6 depicts the predicted hole fraction dependence of thermo-occupancy function at a reduced temperature $\tilde{Y}_h(h, \tilde{T})$ versus the inverse of h at ambient pressure. The universal curve stands for the line of the best fit through the estimated points for all species researched. The curve indicates that the $\tilde{Y}_h$ function of occupancy tends to increase as h decreases as a measure of configurational stability. Greater stability of transportation in the structure is represented by $\tilde{Y}_h$, and consequently infers a more viscous effect.

3.2. Dependence of dynamic viscosity on hole fraction

Section 3.1 described the computation of the SS theory parameters together with the hole fraction for the corresponding pressure and temperature. Now, using the hole fraction results, we predict the viscosity of the hydrocarbons under study via the previously published zero shear viscosity model. More specifically, the discussion is about the viscosity prediction with the fitting parameters and its relation to the vacancy fraction as a particular type of free volume fraction.

The database regarding viscosity is required by the open literature [2, 43]. Temperature and pressure range for viscosity are the same with PVT data as indicated in Table I, namely $298.15 \leq T \leq 473.15$ K and $0.1 \leq P \leq 202.4$ MPa. The viscosity is determined with a vibrating-wire instrument, for which technical details and experimental procedure can be found in [2, 43].

Using the computed thermo-occupancy function, Y_h, comprising the hole fraction, and (9) and (14) allow the prediction of viscosity. The regression

TABLE IV

Rheological parameters of (9) (hole fraction correlation to viscosity) together with data fit statistics.

Hydrocarbons	$\ln(\eta^*)$	α	a' $(\times 10^2)$	κ	$\Delta\eta\%$	R^2
n-octane	−18.93	33.90	0.45	0.027	0.49	0.99996
n-decane	−18.54	37.64	0.37	0.019	0.40	0.99998
n-dodecane	−18.75	44.08	0.38	0.023	0.53	0.99996
n-octadecane	−18.64	64.39	0.37	0.021	0.36	0.99998
1,3-dimethylbenzene (m-xylene)	−19.07	30.51	0.418	0.031	0.42	0.99997
1,2,3,4-tetrahydronaphthalene (tetralin)	−19.03	42.28	0.423	0.030	0.31	0.99999
1-methylnaphthalene (1-MNP)	−19.21	42.97	0.40	0.037	0.47	0.99997

TABLE V

Rheological of parameters of (14) and (15) (hole fraction correlation to viscosity) together with data fit statistics.

Hydrocarbons	h'	$\ln(\eta^*)$	α	a' $(\times 10^2)$	κ	$\Delta\eta\%$	R^2
n-octane	0.64	−19.80	510.20	6.74	0.066	0.17	0.999995
n-decane	0.25	−19.64	280.19	2.78	0.056	0.15	0.999997
n-dodecane	0.2	−19.53	236.30	2.05	0.05	0.24	0.999991
n-octadecane	0.16	−19.32	240.05	1.39	0.041	0.15	0.999997
1,3-dimethylbenzene (m-xylene)	0.7	−19.92	531.09	7.28	0.074	0.19	0.999994
1,2,3,4-tetrahydronaphthalene (tetralin)	0.04	−19.36	80.82	0.80	0.043	0.09	0.999998
1-methylnaphthalene (1-MNP)	0.04	−19.67	89.16	0.83	0.058	0.26	0.999987

quantities established from (9), (11) and (14), i.e., κ and $\ln(\eta^*)$ alongside α and a', are given in Tables IV and V. The statistics of the data fit — namely the coefficient of determination R^2 and the relative mean average percentage error (rMAPE) in viscosity ($\Delta\eta\,[\%]$), determined from

$$\Delta\eta = \frac{1}{N}\sum\nolimits_i \left|1 - \frac{\eta_i^{calc}}{\eta_i^{\exp}}\right| \times 100\%, \tag{20}$$

are also listed in Tables IV and V.

Values for rMAPE, $\Delta\eta\,[\%]$, were calculated for the zero shear viscosity model fits of the viscosity data. The viscosity-hole fraction equations given in (9) and (14) are found to represent the experimental viscosity data of seven hydrocarbons with mean percentage errors as 0.43 and 0.22%, respectively. The correlation incorporated the additional hole fraction h' (see (14)), halved the difference between measurement and model prediction and is found to be more representative of the viscosity data than (9). The results are visible in Tables IV and V.

To elucidate the logarithmic viscosity-thermooccupancy behaviour, the dependence of $\ln(\eta)$ vs Y_h is shown in Figs. 7 and 8, and in Figs. 9 and 10, the dependence of $\ln(\tilde{\eta}_0)$ vs $\tilde{Y}_h$ is plotted for the materials studied. The lines correspond to the best approximation of the data set for each hydrocarbon. On the line, the pressure goes up from the lower to upper part for each temperature, and while regarding any fixed pressure data, temperature drops as going higher. At the lower part of the lines where pressure drops and temperature rises, the lines are converging, whereas at the upper part, they are diverging. As going down through the line, higher temperature and lower pressure give rise to the amount of hole fraction and result in the easy accumulation of molecules in the nanovoids. With regard to this effect, it is not easy to distinguish the materials at this part in Figs. 9 and 10. Conversely, as going to a lower temperature and higher pressure, the free volume and hole fraction decrease produce less transportation of molecules, especially the ones with longer chain length and more ring attached structures since they occupy larger free volume. In Figs. 7 and 8 the viscosity of linear alkanes are in the following order: n-octadecane $>$ n-dodecane $>$ n-decane $>$ n-octane. Figure 7 shows that, as anticipated, m-xylene is the lowest viscous material in the aromatics.

As it is shown in Fig. 7, (9) provides a good linear fit to $\ln(\eta)$ vs Y_h data. Since the lines and data are slightly telescoped in the graph for the studied hydrocarbons, it is better just to look at Table IV to check the value of the correlation coefficient squared R^2, which has an excellent agreement with $R^2 \geq 0.9999$. Another example is shown in Fig. 8, where the parameter in the denominator of Y_h in (14) and (15) is taken as $h' \neq 0$. Better fits were observed in the latter. When $\Delta\eta\,[\%]$ is halved, there is an improvement in the fifth decimal of the values of R^2 in Table V compared to Table IV. The linearisation parameter h' seems to change from material to material, and contrary to our expectations decreases with the chain length for n-alkanes, as seen in Table V in this study. It seems to be the

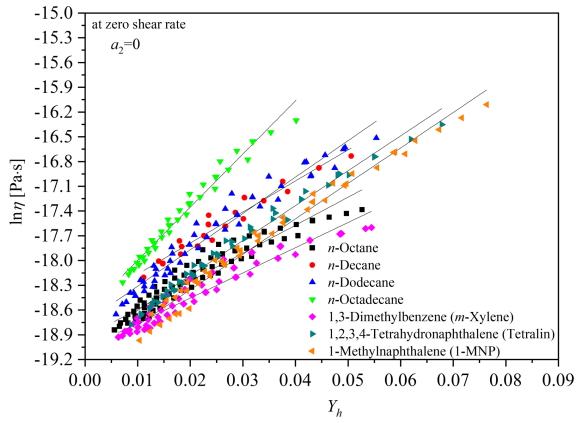

Fig. 7. Linearisation of $\ln(\eta)$–Y_h dependence by means of (9).

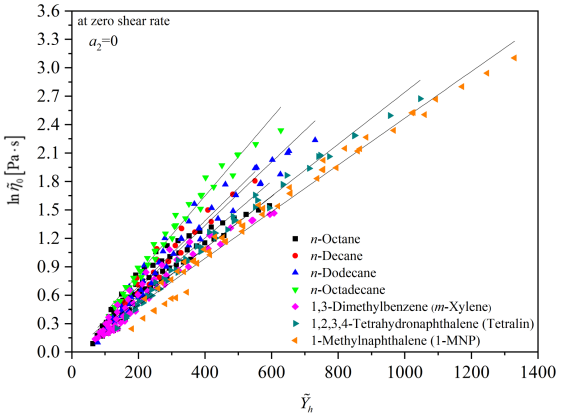

Fig. 9. Linearisation of $\ln(\tilde{\eta}_0)$–$\tilde{Y}_h$ dependence by means of (10).

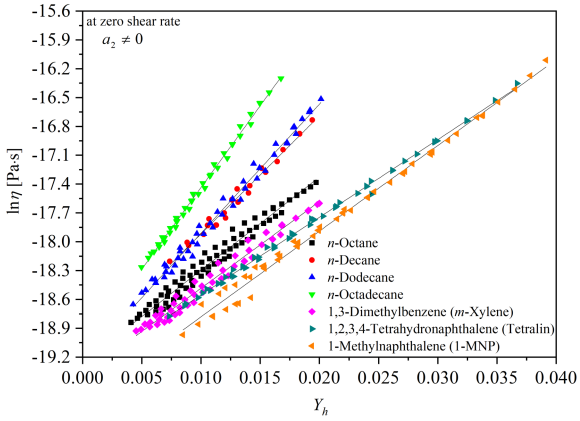

Fig. 8. Linearisation of $\ln(\eta)$–Y_h dependence by means of (14) and (15).

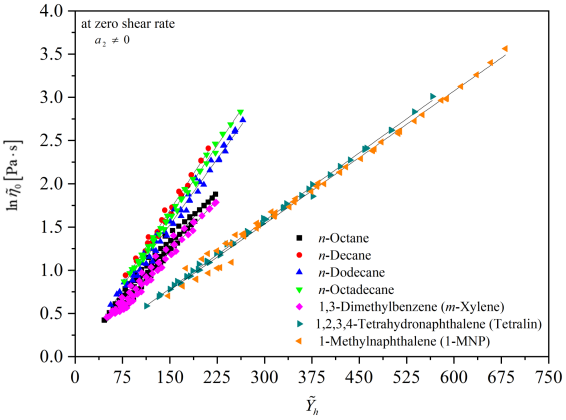

Fig. 10. Linearisation of $\ln(\tilde{\eta}_0)$–$\tilde{Y}_h$ dependence by the use of (16) and (17).

result of the high assigned values ($0.2 \leq h' \leq 0.7$), except of tetralin and 1-MNP ($h' = 0.04$). On the other hand, in one of the previous papers [18] the values of h' were in the lower range, from 0.002 to 0.075, and ascended with increasing carbon number of an alkane as expected. In the paper reported by Yahsi [17], h' was found to be around 0.06 for linear, and 0.09 for the three-branched alkanes.

Since α has similar values across some pair of species in Table V (*n*-octane/1,3-dimethylbenzene (*m*-xylene), *n*-decane/*n*-dodecane/*n*-octadecane and 1,2,3,4-tetrahydronaphthalene (tetralin) /1-methylnaphthalene (1-MNP)), we demonstrated the scaled form of viscosity in Figs. 9 and 10. In Figs. 9 and 10, $\ln(\tilde{\eta}_0)$ is plotted as a function of $\tilde{Y}_h$ with $h' = 0$ and $h' \neq 0$ according to (10), (13) and (16), (17). At a given temperature and pressure $\ln(\tilde{\eta}_0)$ steps up linearly with $\tilde{Y}_h$ since the latter function is inversely proportional to the hole fraction.

Now, we wanted to see whether α, h', a' are interrelated. As stated above, as Y_h and $\tilde{Y}_h$ incoming from (9), (10), (14) and (16) increase, the differences in viscosities become more apparent. This variation is acquired from the slopes of the lines in Figs. 7–10, yielding the values of α — the measure of activation energy. Concerning the α values in Table IV, the graph of α vs segment number s is shown in Fig. 11. It is visible that as the value of s number goes up, both *n*-alkanes and aromatics exhibit larger slopes, α. This demonstrated that for *n*-alkanes the segment number is the indicator for the viscous degree. In addition to that, for the aromatics, the viscosity increases as well, as going to mono- to di-aromatics. In other words, the viscosity increases with the number of aromatic rings. From the outcomes of species under investigation, the ranked increase in the measure of activation energy coefficient, α, emerges as *n*-octadecane > *n*-dodecane> *n*-decane > *n*-octane and 1-MNP > tetralin > *m*-xylene for *n*-alkanes and aromatics, respectively. This result is in accordance with that of $\langle \varepsilon^* \rangle$ discussed above. In (11), the activation energy quantity a' is computed and listed in Tables IV and V. It is found to be around 0.004 without significant difference in Table IV, and no systematic relation is observed across the species (Fig. 12), it is even expected to be increased with segment number, like

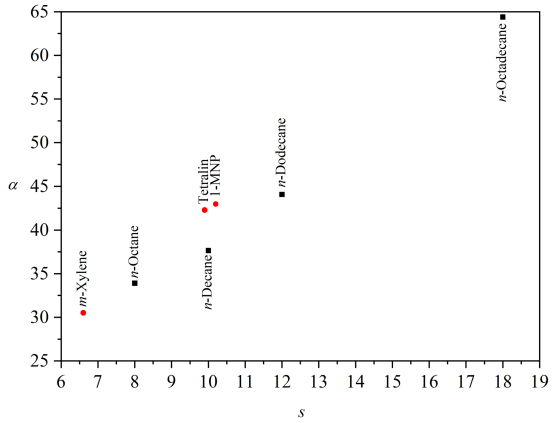

Fig. 11. The segment number dependence of α reckoned by (9) for the materials in Table I.

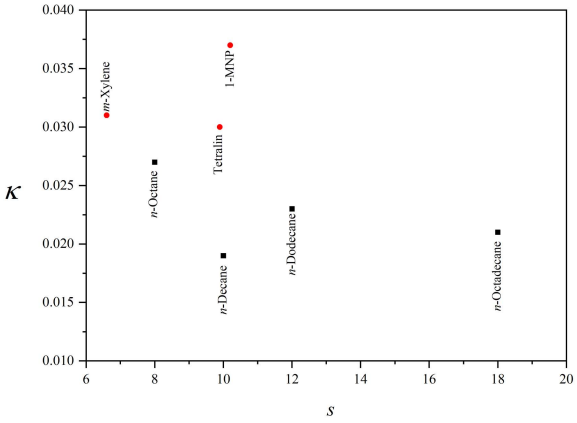

Fig. 13. The segment number dependence of determined κ through (9) and (11) for the materials in Table I.

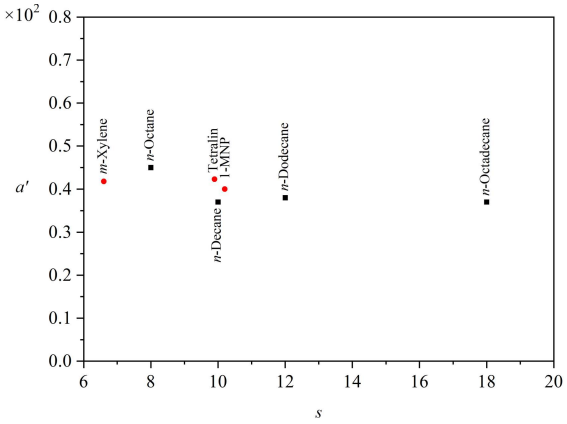

Fig. 12. The segment number dependence of reckoned a' by means of (9) and (11) for the materials in Table I.

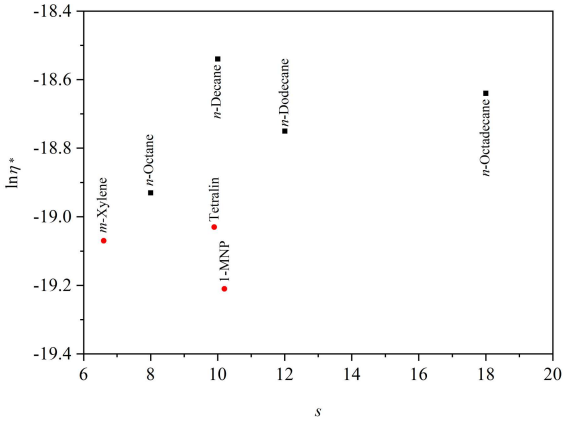

Fig. 14. The segment number dependence of determined $\ln(\eta^*)$ by the use of (9) for the materials in Table I.

the measure of activation energy coefficient [17, 18]. In Table V, the measure of activation energy, α, is lower for n-dodecane than n-octadecane (with similar h' values), as well as lower for tetralin than 1-MNP. Tetralin and 1-MNP have equal and low h' values, so both α and a' increase as going from tetralin to 1-MNP, even if for a' the increase is only negligible. For n-alkanes (n-decane, n-dodecane, n-octadecane), except for n-octane, the assigned h' parameters are in a close proximity to each other, and found around 0.2. The samples, namely n-octane and 1,3-dimethylbenzene, have higher h' values that adversely affect the systematic behaviour of the parameters for not only α and a', but also κ and $\ln(\eta^*)$ listed in Table V, as was explained in the preceding section. Hence, the behaviour of α and a' parameters for the materials with a close or equal number of h' is compatible with the results obtained before [17, 18].

Actually, for each species different h' parameters were adjusted, except for tetralin and 1-MNP. These values have been obtained to be decreased as the segment number increases, except for the last two in Table IV. Since α, a' and h' have similar behaviour according to the chain length [17, 18], and h' decreases with the chain length in this study, the general decreasing behaviour for α and a' with chain length is straightforward according to Table V. This is why it would be better to take for comparison the fixed h', when its value is similar for all studied species. However, our adjusted h' is, in general, found different across the materials, and difficult to be taken as a fixed value, in contrast to the previous findings [4, 6, 7, 10, 17]. Yahsi found a slightly higher relative deviation when he employed h' as an Utracki's fixed value than the adjusted one [16].

According to Tables IV and V, the transmission coefficient, κ and $\ln(\eta)^*$, coming from (9), (11) and (14) are inversely related to each other (see (11)). In Table IV and Fig. 13, κ decreases with chain length, except for some species across n-alkanes and aromatics. Concerning $\ln(\eta^*)$ in Table IV and Fig. 14, it increases with segment number across hydrocarbons, with only a few exceptions. Contrary

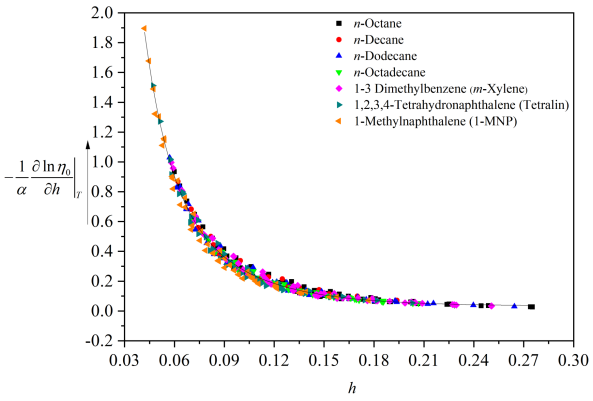

Fig. 15. The dependence of $(-1/\alpha)(\partial \ln \eta_0/\partial h)|_T$ vs h using (18) for the hydrocarbons under study.

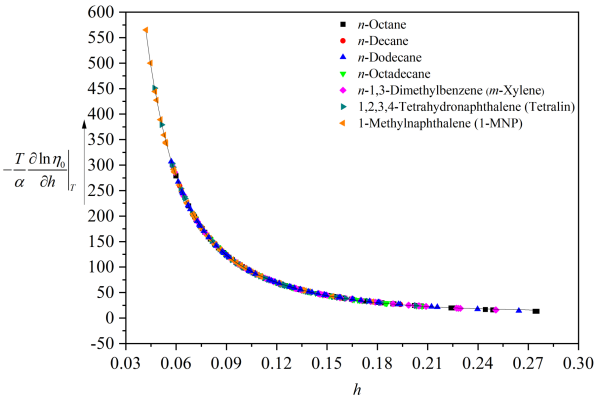

Fig. 16. The dependence of $(-T/\alpha)(\partial \ln \eta_0/\partial h)|_T$ vs h using (18) for the hydrocarbons under study.

to the expectations [21, 22], κ decreases and $\ln(\eta)^*$ increases with s number. As the hole fraction increases depending on high temperature and low pressure, there would be no contribution to the viscosity from Y_h as seen from (9) and (14). In this case, $\ln(\eta)$ would be equal to viscosity intercepts $\ln(\eta)^*$. The materials with higher viscosity produce larger free volume at elevated temperature and low pressure states, and eventually have the less viscous effect (viscosity intercepts $\ln(\eta)^*$). This enables the molecules to migrate into the holes and results in an increase in the probability of the transmission with κ, values of which range from 0 to 1. The more obvious pattern referring to this concern can be seen in Table V. From among all the n-alkanes in Table V, κ steps down and $\ln(\eta)^*$ increases with chain length, without any exceptions since the assigned hole fraction parameters (h') are large in magnitude and fall with segment numbers for each material. As stated above, the decreasing trend in the assigned large values of h' with carbon numbers further enables the unusual change in κ and $\ln(\eta)^*$ behaviour. In the case where equal and low hole fraction parameter h' is assigned for the last two aromatics in Table V, κ increases with chain length as going mono- (tetralin) to di-aromatics (1-MNP) (see Table IV). This is because, from tetralin to 1-MNP, with the condition of high temperature and low pressure, the hole fraction increase allows transporting more molecules into the holes. In contrast, $\ln(\eta)^*$ decreases from tetralin to 1-MNP since high temperature and low pressure leads to excessive hole fraction.

The graphical representation of the differentiation of logarithm of viscosity (viscoholibility) vs hole fraction in Fig. 15, expresses the viscosity change according to vacancy fraction function h, at constant T, as the fraction h varies on the abscissa axis. Dividing viscoholibility given in (18) by the structure-related parameter, $-\alpha$, defined in (11), overlaps the full data on the ordinate axis. The solid curve represented by $(\partial \ln(\eta_0)/\partial h)|_T = -\alpha\,[18.01 - 15.748(1 - \exp(-h/0.015)) - 2.23(1 - \exp(-h/0.044))]$ characterises the exponential fit through the data. In Fig. 15 it is clear that at the lower values of h, the derivative function for logarithmic viscosity vs h reliance, switches to abruptly lower points. Particularly, the viscoholibility diminishes by a factor of five when the hole fraction is nearly doubled. After a point $h \simeq 0.08$, we observe only a slight change in the derivative function and the viscoholibility steps down monotonously with a hole fraction, although the fit has a small negative curvature. Additionally, the decrease of viscoholibility is systematically less and less pronounced, and descends almost linearly with a rising hole fraction. It saturates at about $\simeq 0.032\alpha$ and remains nearly stable in the range where hole fraction is in excess. In order to remove the scatter in Fig. 15, the viscoholibility on the vertical axis is multiplied by temperature T considering the thermal energy of molecules (see Fig. 16).

4. Conclusion

The behaviour of PVT and the dynamic viscosity of seven hydrocarbons with two different chemical families, four of which are n-alkanes and three are aromatics, were examined by the means of a zero shear viscosity model. The formalism incorporates hole fraction parameter reckoned by the Simha–Somcynsky equation of state (SS-EoS). In this treatise, the main findings can be outlined as follows:

1. The material-dependent pressure, volume and temperature parameters (P^*, V^*, and T^*) together with the interaction parameters (υ^*, ε^*) are determined using the SS lattice-hole theory. Longer chained hydrocarbons have higher characteristic attractive interaction energy parameters ε^*, and lower repulsive molar volume parameters υ^* than the shorter chained hydrocarbons. Besides, di-aromatics have higher ε^* and lower υ^* values compared to mono-aromatics.

2. The characteristic volume (V^*) parameters are lower for n-alkanes with more carbon numbers and di-aromatics, while the characteristic pressure (P^*) parameters are higher. In the case of V^*, it shows similar characteristics with υ^*, and P^* with ε^*.
3. Our previously published physically-based zero-shear viscosity model comprising the thermo-occupancy function Y_h confirms that the viscosity is correlated reciprocally to hole fraction. Accordingly, the logarithmic viscosity of the individual hydrocarbons shows a linear relationship (at several temperatures and pressures) with T and h dependent thermo-occupancy function Y_h. The viscoholibility, differential form of viscosity referred to as the derivative of logarithmic viscosity with respect to h, diminishes with increasing fraction h.
4. The n-alkanes possessing fewer carbon numbers and mono-aromatics, appear to have the smaller activation energy measure α — the slope of the lines in the logarithm of viscosity versus Y_h. Longer chained n-alkanes have greater α values than the shorter chained n-alkanes, and di-aromatics possess larger α values than mono-aromatics. The result obtained for α is similar to ε^* since both parameters are inversely related to the distance between segments.
5. The values of hole fraction h are greater for the groups of both mono-aromatics and fewer carbon numbers of n-alkanes. The findings for the Y_h function are in reverse with that of h. Conceptually, the lower hole fraction values increase viscosity, while decreased Y_h reduce it. Consequently, the longer chained n-alkanes have higher viscosity effects than fewer carbon numbers of n-alkanes, while di-aromatics have stronger viscosity effects than mono-aromatics.

Acknowledgments

This work did not receive any specific grant from funding organisations in the public, commercial, or non-profit sectors.

References

[1] X. Canet, P. Daugé, A. Baylaucq, C. Boned, C.K. Zéberg- Mikkelsen, S.E. Quińones-Cisneros, E.H. Stenby, *Int. J. Thermophys.* **22**, 1669 (2001).

[2] D.R. Caudwell, J.P.M. Trusler, V. Vesovic, W.A. Wakeham, *J. Chem. Eng. Data* **54**, 359 (2009).

[3] J.S. Dickmann, J.C. Hassler, E. Kiran, *J. Supercrit. Fluid* **98**, 86 (2015).

[4] L.A. Utracki, *J. Rheol.* **30**, 829 (1986).

[5] A.K. Doolittle, *J. Appl. Phys.* **22**, 1471 (1951).

[6] L.A. Utracki, *Can. J. Chem. Eng.* **61**, 753 (1983).

[7] L.A. Utracki, *Polym. Eng. Sci.* **23**, 446 (1983).

[8] L.A. Utracki, *J. Appl. Polym. Sci.* **84**, 1101 (2002).

[9] L.A. Utracki, T. Sedlacek, *Rheol. Acta.* **46**, 479 (2007).

[10] L.A. Utracki, *Polym. Eng. Sci.* **25**, 655 (1985).

[11] S.E. Kadijk, B.H.A.A. Vandenbrule, *Polym. Eng. Sci.* **34**, 1535 (1994).

[12] L.A. Utracki, *Adv. Polym. Technol.* **7**, 35 (1987).

[13] T. Sedlacek, R. Cermak, B. Hausnerova, M. Zatloukal, A. Boldizar, P. Saha, *Int. Polym. Proc.* **20**, 286 (2005).

[14] E. Rojo, M. Fernandez, M.E. Munoz, A. Santamaria, *Polymer* **47**, 7853 (2006).

[15] A. Sorrentino, R. Pantani, *Rheol. Acta* **48**, 467 (2009).

[16] U. Yahsi, *Polym. Eng. Sci.* **38**, 464 (1998).

[17] U. Yahsi, *J. Polym. Sci. Pol. Phys.* **37**, 879 (1999).

[18] U. Yahsi, F. Sahin, *Rheol. Acta* **43**, 159 (2004).

[19] F. Sahin, C. Tav, U. Yahsi, *Int. J. Thermophys.* **27**, 1501 (2006).

[20] F. Sahin-Dinc, *Intern. Polym. Process.* **30**, 585 (2015).

[21] F.S. Dinc, T. Sedlacek, C. Tav, U. Yahsi, *J. Appl. Polym. Sci.* **131**, 40540 (1) (2014).

[22] F. Sahin-Dinc, A. Sorrentino, C. Tav, U. Yahsi, *Int. J. Thermophys.* **36**, 3239 (2015).

[23] F. Sahin-Dinc, U. Yahsi, T. Sedlacek, *Adv. Polym. Technol.* **2019**, 1 (2019).

[24] M.J. Assael, M. Papadaki, W.A. Wakehan, *Int. J. Thermophys.* **12**, 449 (1991).

[25] A. Baylaucq, C. Boned, P. Dauge, B. Lagourette, *Int. J. Thermophys.* **18**, 3 (1997).

[26] A. Et-Tahir, C. Boned, B. Lagourette, P. Xans, *Int. J. Thermophys.* **16**, 1309 (1995).

[27] J.S. Chang, M.J. Lee, *J. Chem. Eng. Data* **40**, 1115 (1995).

[28] H. Kashiwagi, T. Makita, *Int. J. Thermophys.* **3**, 289 (1982).

[29] W.A. Burgess, D. Tapriyal, B.D. Morreale, Y. Wu, M.A. McHugh, H. Baled, R.M. Enick, *Fluid Phase Equilib.* **319**, 55 (2012).

[30] C. Boned, C.K. Zéberg-Mikkelsen, A. Baylaucq, P. Daugé, *Fluid Phase Equilib.* **212**, 143 (2003).

[31] R. Simha, T. Somcynsky, *Macromolecules* **2**, 342 (1969).

[32] L.A. Utracki, M. Sepehr, J. Li, *Int. Polym. Proc.* **21**, 3 (2006).

[33] J.S. Dickmann, M.T. Devlin, J.C. Hassler, E. Kiran, *Ind. Eng. Chem. Res.* **57**, 17266 (2018).

[34] U. Yahsi, B. Coskun, A. Yumak, K. Boubaker, C. Tav, *Eur. Polym. J.* **68**, 226 (2015).

[35] U. Yahsi, K. Ulutas, C. Tav, D. Deger, *J. Polym. Sci. Pol. Phys.* **46**, 2249 (2008).

[36] U. Yahsi, H. Deligöz, C. Tav, K. Ulutaş, D. Değer, S. Yılmaztürk, G. Erdemci, B. Coşkun, M. Yılmazoğlu, Ş. Yakut, *Radiat. Eff. Defects Solids* **174**, 214 (2018).

[37] T.S. Ree, T. Ree, H. Eyring, *Proc. Natl. Acad. Sci. USA* **48**, 501 (1962).

[38] T.S. Ree, T. Ree, H. Eyring, *J. Phys. Chem.* **68**, 3262 (1964).

[39] S. Glasstone, K.L. Laidler, H. Eyring, *The Theory of Rate Processes; the Kinetics of Chemical Reactions, Viscosity, Diffusion and Electrochemical Phenomena*, McGraw-Hill Book Company, New York, 1941.

[40] T.S. Ree, H. Eyring, T. Ree, *P. Natl. Acad. Sci. USA* **51**, 344 (1964).

[41] T.S. Ree, T. Ree, H. Eyring, *J. Phys. Chem.* **68**, 3262 (1964).

[42] H. Eyring, *J. Chem. Phys.* **4**, 283 (1936).

[43] D.R. Caudwell, J.P.M. Trusler, V. Vesovic, W.A. Wakeham, *Int. J. Thermophys.* **25**, 1339 (2004).